10 Feb 2022

Dynamical Properties of Environmental High-Performance Composites with Calcined Clay

Jingjie Wei

Wu Jian Long

Kamal Khayat
Missouri University of Science and Technology, khayatk@mst.edu

Biqin Dong

et. al. For a complete list of authors, see https://scholarsmine.mst.edu/civarc_enveng_facwork/2358

Recommended Citation

J. Wei et al., "Dynamical Properties of Environmental High-Performance Composites with Calcined Clay," *Journal of Cleaner Production*, vol. 335, article no. 130226, Elsevier, Feb 2022.
The definitive version is available at https://doi.org/10.1016/j.jclepro.2021.130226

Journal of Cleaner Production 335 (2022) 130226

Contents lists available at ScienceDirect

Journal of Cleaner Production

journal homepage: www.elsevier.com/locate/jclepro

Dynamical properties of environmental high-performance composites with calcined clay

Jingjie Wei [c,d], Wu-Jian Long [a,b,c,*], Kamal H. Khayat [d], Biqin Dong [a,b,c], Liu Mei [a,b,c], Feng Xing [a]

[a] Guangdong Provincial Key Laboratory of Durability for Marine Civil Engineering, Shenzhen, 518060, Guangdong, PR China
[b] Key Lab of Coastal Urban Resilient Infrastructure, MOE, Shenzhen University, Shenzhen, 518060, Guangdong, PR China
[c] College of Civil and Transportation Engineering, Shenzhen University, Shenzhen, 518060, Guangdong, PR China
[d] Department of Civil, Architectural and Environmental Engineering, Center for Infrastructure Engineering Studies, Missouri University of Science and Technology, Rolla, MO, 65401, USA

ARTICLE INFO

Handling Editor: Zhen Leng

Keywords:
High-performance composite
Limestone calcined clay cement
Calcined clay
Dynamic property
Microstructure
Ecological benefit

ABSTRACT

Concrete structures may be exposed to dynamic loadings within short periods such as earthquakes and vehicles load, resulting in substantial damage to human life and property because of the collapse of concrete structures. The research achievements on dynamic properties of high-performance composites with LC^3 (HPC-LC^3) are limited, although dynamic loadings are commonly encountered in infrastructure. The study aims to develop a new-green concrete product (HPC-LC^3) with high dynamical properties and promote its mass use in a vibration service environment by investigating dynamical properties of HPC-LC^3. Dynamical properties of structure can be promoted at material level by means of enhancing the inherent ability of cement-matrix materials to passively absorb the vibrational energy. Dynamic properties of traditional HPC may be improved by incorporated LC^3 because of excellent mechanical properties. The fiber pull-out, thermogravimetric analysis (TGA), (nuclear magnetic resonance) NMR, and microstructure test were used to reveal the enhanced mechanism of dynamic properties in the HPC with LC^3 (HPC-LC^3), and the economic efficiency of HPC is also evaluated to promote its mass application. The results indicate that the dynamic properties of HPC-LC^3 increased by 47% in damping capacity, 102% in storage modulus, 16% in energy dissipation, in comparison with the reference (HPC-OPC). Meanwhile, compared with the reference, the compressive and flexural strengths of LC^3-50 increased by 14% and 27%. TGA and NMR results indicate that LC^3-50 shows better hydration characteristics, longer alumina-silicate chain length (from 3.9 to 8) than HPC-OPC. The proposed composites reduced embodied energy, embedded CO_2 emissions, and costs of HPC by up to 33%, 45%, and 7%, respectively. Thus, the green product (HPC-LC^3) with 30%–40% calcined clay, high dynamic properties and more sustainable, will be recommended to mass use in a vibration service environment.

1. Introduction

High-performance composites (HPC) are advanced cementitious composites with outstanding performance, compared to conventional cementitious materials (Meng et al., 2018). HPC contains a high proportion of Portland cement (800–1300 kg/m^3), which releases large amounts of CO_2 (Wang et al., 2018). The high proportion of Portland cement in HPC, large amount of CO_2 emission and economic cost increase, are the primary factors limiting its widespread application. As researchers have become more attentive to the energy consumption surging from 17.67 billion GJ to 109.9 billion GJ in China (Yuan et al., 2015), specially that building and transportation sector is one of the largest energy consumers (Zhou et al., 2016). The negative environmental effects of building materials have been revealed, stimulating investigations into the development of green binder systems to reduce the environmental impact of HPC.

Based on previous investigations, with regarding to the reduction of environmental impact and cost, as well as saving performance, cement

Abbreviations: BSEM, Backscattered scanning electron microscopy; DMA, Dynamic mechanical analyzer; ECO_2e, Embedded CO_2 emissions; EE, Embodied energy; LC^3, Limestone calcined clay cement; MIP, Mercury intrusion porosimetry; OPC, Ordinary Portland cement; SCMs, Supplementary cementitious materials; HPC, High-performance composites.

* Corresponding author. College of Civil and Transportation Engineering, Shenzhen University, Shenzhen, 518060, Guangdong, PR China.
E-mail address: longwj@szu.edu.cn (W.-J. Long).

https://doi.org/10.1016/j.jclepro.2021.130226
Received 4 April 2021; Received in revised form 12 December 2021; Accepted 19 December 2021
Available online 22 December 2021

can be appropriately replaced by supplementary cementitious materials (SCMS), such as fly ash (Yu et al., 2020) and kaolinitic clays (Alujas et al., 2015), in modern concrete technology. A reduction in sources and increased consumption of industry byproducts has restricted the availability of commonly used SCMs (Snellings, 2016). With the rapid development of the construction industry, the quality of raw materials in HPC must be strictly controlled to ensure the high levels of performance for filed applications (Gursel et al., 2016). Some SCMs are costly, especially rice husk ash and silica fume. For all these reasons, the industry currently seeks new alternative cementitious materials that offer good performance, cost efficiency, and reduced environmental impact.

Calcined clay, obtained after burning raw clay at temperatures of 650–800 °C, exhibits high pozzolanic activity (Scrivener et al., 2018). It is a widely spread material in the world, cheap and easily accessible, as well as quite suitable for developing countries. Studies reported that calcined clay has been utilized as a cement substitute in concrete production (Avet et al., 2018) and is more widely available than other SCMs (Yu et al., 2020). For example, Alujas et al. (2015) indicates that calcined clay with moderate contents of kaolinite constitute a potential source of high reactivity pozzolanic materials. Based on the investigation from Scrivener et al. (2018), limestone calcined clay cement (LC^3), consisted of calcined clay, limestone, clinker and gypsum, can significantly improve the performance of concrete than single use of calcined clay. For example, LC^3 exhibited good mechanical performance (Avet et al., 2018), adequate mitigation of alkali-silica reactions with reactive aggregates (Nguyen et al., 2020), suitable performance in the presences of sulfates, and excellent resistance to chloride penetration (Yang et al., 2020). Although most studies focused on fresh properties, static mechanical properties, durability of mixtures mixed with LC^3, there is limited research achievements on the dynamic properties of HPC with LC^3.

Structures may be exposed to dynamic loadings within short time periods such as earthquakes and vehicles load during their service life. The damage of structures caused by earthquakes is abrupt and causes substantial damage to human life and property. The dynamic properties of Portland cement were lower (Chi et al., 2019). Based on previous studies, dynamical properties can be promoted at material level by means of enhancing the inherent ability of cement-matrix materials to passively absorb the vibrational energy. Dynamic properties of the cement-matrix composites depend partially on each constituent and matrix microstructure. For example, Chung (2000, 2002); Fu et al. (1998); Fu and Chung (1996) investigated the effect of silica fume, cement, and sand on damping and stiffness on pure slurry, mortar, and concrete. The results showed that silica fume can improve the dynamic properties of cement paste, and sand decreases storage modulus while increases the damping ability of mortar. According to previous literature, graphene (Muthusamy et al., 2010), graphene oxide nanosheets (Lv et al., 2014), and polymer (Kwon et al., 2019), and carbon nanotube (Liew et al., 2017), as well as asphalt (Yuan et al., 2016) could improve the damping ability of concrete material significantly. Fang et al. (2017) investigated the effects of key mix parameters, including water–cement ratio (W/C) and sand–cement ratio (S/C), on the dynamic properties of the mortar, showing that storage modulus increased with increased S/C ratio and decreased W/C ratios, damping ability of mortar increased with increased in W/C ratios. Chi et al. (2019) summarized the effect of different materials, such as recycled rubber aggregate, and fiber on dynamic properties indicating micro-particle damping and interlocking damping microstructural engineering are very promising in the future.

The previous studies are focusing on dynamic properties of conventional cement-based composites (OPC). The use of conventional cement-based composites releases a large amount of CO_2 emission, although the dynamic properties of concrete can be improved slightly by suitable design. However, the improvement of dynamic properties for conventional cement-based composites is limited due to physical and chemical property of conventional binder system and mixture proportion. As a result, a new cement binder system should be developed to show high dynamic properties as well as low CO_2 emission. LC^3 present an extremely promising option to achieve lower CO_2 emissions and lower costs. Most studies focused on fresh properties, static mechanical properties, durability of cement-based composites incorporating with LC^3. The research achievements on dynamic properties of HPC with LC^3 are limited. According to Scrivener et al. (2018) reported, the different dosage of calcined clay showed significant effect on performance of cement-based composites. The dosage of calcined clay should also be investigated for better dynamical behavior of HPC incorporated with LC^3.

For the sustainable use of HPC in a vibration service environment, it is urgently necessary to identify dynamical properties of low-carbon HPC made with different mixture proportion. The study aims to develop a new-green concrete product (HPC-LC^3) with high dynamical properties and low CO_2 emission by investigating static and dynamical properties of HPC-LC^3. The thermogravimetric analysis (TGA), nuclear magnetic resonance spectroscopy (NMR) as well as microstructural properties, were investigated to reveal the enhanced mechanism of HPC-LC^3 in dynamic properties. To promote the green concrete product mass use in filed application, the environmental impact and economic cost of each mixture were investigated by life cycle assessments. The HPC-LC^3 mixed with optimized calcined clay dosage, exhibited better dynamical properties and provided environmental and economic benefits, was recommended to use in a vibration service environment.

2. Materials and methods

The physical and chemical properties of different ingredients used to prepare the HPC samples are discussed in Sections 2.1, 2.2, and 2.3. The mixture proportion and procedure for preparing samples is discussed in Section 2.4. Different methods are designed, in Section 2.5, to understand the effect of different binder proportions on performance of HPC. For example, mercury intrusion porosimetry (MIP) was used to reveal the enhanced mechanism of mechanical performance.

2.1. Supplementary cementitious materials (SCMs) and cement

In this study, SCMs and cement (42.5R) were used in accordance with the Chinese standard (GB/T175-2007). The SCMs were limestone filler, gypsum, and calcined clay. The chemical compositions of the SCMs and cement are presented in Table 1. The physical properties of the cement are shown in Table 2. The particle size distributions of SCMs and the cement shown in Fig. 1 were determined by a laser particle size analyzer.

2.2. Fine aggregate and steel fiber

The fine aggregate used in this study was natural river sand, which was obtained from Xiamen ISO standard sand Co., Ltd (Xiamen city, China). The aggregate was to conform to the properties required in the Chinese standard (GB/T 14684). The aggregate had a maximum particle size of 4.75 mm and fineness modulus of 3.0. The physical characteristics is shown in Table 3. A brass-coated steel fiber with a diameter of 0.2 mm and length of 13 mm was selected for investigation. The tensile strength of the selected fiber was around at 2790 MPa.

2.3. Mixing water and chemical admixture

Ordinary tap water was selected as the mixing water, which is conformed to JGJ63-2006. To ensure the workability of HPC, the polycarboxylate superplasticizer (PCE) produced by Sika was used, and a maximum water-reducing ability is between 30 and 35%, which is in accordance with the requirements of JG/T 223-2007 (2007).

Table 1
Chemical composition of cement and SCMs (mass%).

Component	CaO	SiO_2	Al_2O_3	Fe_2O_3	MgO	SO_3	K_2O	Na_2O	LOI
Cement/Clinker	64.42	20.52	5.62	3.78	2.11	2.10	0.28	0.29	0.88
Calcined clay	0.3	64.20	28.51	0.65	0.14	0	0.25	0.10	5.40
Limestone	46.21	12.54	3.55	2.56	1.95	0	0.63	0.58	31.98
Gypsum	35.64	4.79	0.60	0.58	1.48	38.77	0.05	0.07	18.02

Table 2
Physical and mechanical properties of cement (ground clinker).

Specific surface area (m^2/g)	ρ_0 (g/cm^3)	Setting time (min)		Flexural strength (MPa)		Compressive strength (MPa)	
0.581	3.00	Initial setting	Final setting	3d	28d	3d	28d
		112	145	4.5	6.2	30.8	44.0

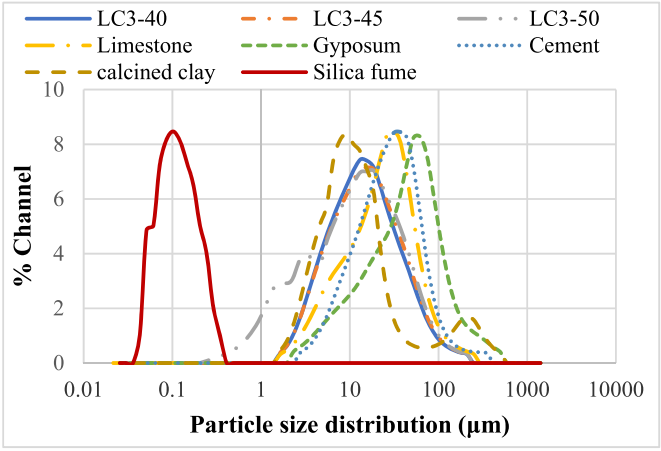

Fig. 1. Particle size distribution of SCMs, cement, LC^3.

2.4. Mixture proportion and specimen preparation

This study focused on the influence of the calcined clay in the LC^3 on dynamic mechanics properties and environmental effect of HPC. Based on the previous study (Scrivener et al., 2018), the content of ground clinker and calcined clay was paid more attention in this study due to considering the environmental effect. The mix proportions of HPC specimens and different mixtures of LC^3 fabricated in this study are listed in Table 4 and Table 5, respectively. Based on the results of previous studies (Meng et al., 2018), the water-to-binder ratio for HPC is between 0.14 and 0.27, and the fineness of calcined clay, limestone, and gypsum results in a large amount of free water absorbed. To ensure the slump flow of HPC, 0.20 was chosen for the water/cement ratio (w/c).

The mixtures were blended by using a high-shear mixer (Type: NA-160A) produced by Jiangsu Wuxi Jianyi Company. The mixing sequences followed previous research, such as Meng et al. (2017). The mixing proceeded as follows: SCMs and sand were mixed for 2 min at a low speed; mixing water and SP were premixed for 4 min which includes 3 min at low speed and 1 min at a high speed; steel fibers were slowly introduced mixed for 3 min at low speed.

HPC was poured into a mini-slump cone for slump flow tests. HPC mixture was cast into 40 × 40 × 160 mm^3 moulds, 50 mm^3 cubes, and 30 mm^3 customized cubic moulds for flexural and compressive strengths tests, and dynamic mechanical analysis test, respectively. The dimension of SEM samples was 10 mm^3, cutting from 30 mm^3 sample for dynamic test. Specimens were kept at standard curing room (20 °C, relative humidity 〉 95%) for almost 24 h, and then they were de-moulded and cured until 28-day.

2.5. Experimental methodologies

Dynamical properties of structure casted by traditional cementitious materials are inherently poor (Chi et al., 2019), and it can be promoted at material level by enhancing inherent ability of cement-matrix to absorb the vibrational energy (Fang et al., 2017). Dynamic properties of traditional HPC may be improved by incorporated LC^3 because of its excellent mechanical properties. Different methodologies are used to investigate dynamical properties of LC^3 with different calcined clay dosages. As shown in Fig. 2, a flow diagram for the overall methodology is added to enhance the reader comprehension.

Table 5
Mixture of ground clinker, calcined clay, limestone, and gypsum (mass %).

Row	Ground clinker	Calcined clay	Limestone	Gypsum
LC^3-50	50%	35%	10%	5%
LC^3-45	45%	40%	10%	5%
LC^3-40	40%	45%	10%	5%

Note: LC^3-X, X means that the percentage of clinker content.

Table 3
Physical characteristics of river sand.

Fine aggregate	Apparent density (kg/m^3)	Bulk density (kg/m^3)	Compact density (kg/m^3)	Void fraction (mass %)	Specific gravity	Crushing value (%)	Water absorption (%)
River sand	2630	1490	1580	40	2.63	–	0.55

Table 4
Mix proportions of HPC.

Mix ID	W/B	N/B	LC^3 (kg/m^3)	Cement (kg/m^3)	Silica fume (kg/m^3)	Natural river sand (kg/m^3)	Water (kg/m^3)	SP (kg/m^3)	Steel fiber (kg/m^3)
OPC	0.2	1.0	–	863	216	1079	194.2	43.2	156
LC^3-50	0.2	1.0	863	–	216	1079	194.2	43.2	156
LC^3-45	0.2	1.0	863	–	216	1079	194.2	43.2	156
LC^3-40	0.2	1.0	863	–	216	1079	194.2	43.2	156

Note: W/B = Water/Binder; N/B = Natural river sand/Binder; SP = Superplasticizer.

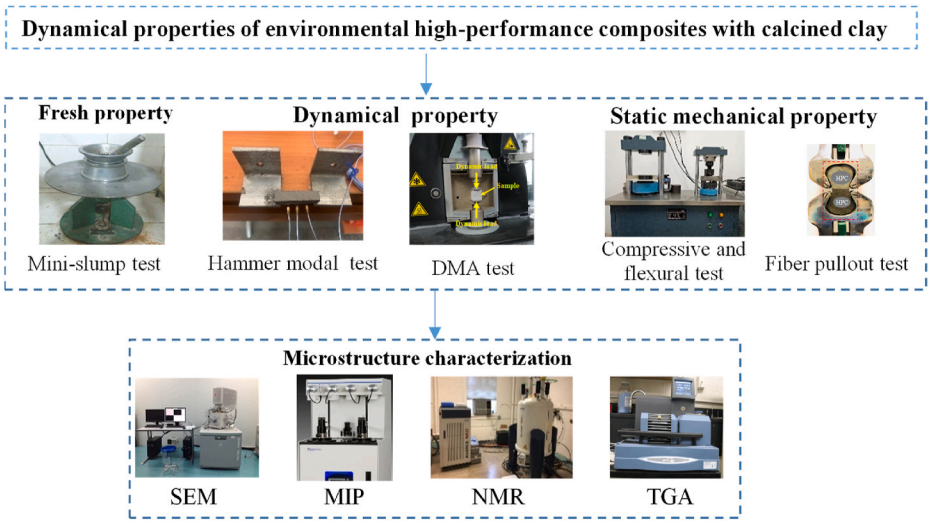

Fig. 2. A flow diagram for the overall methodology.

2.5.1. Mini-slump testing

The flowability and consistency of concrete plays a vital role in ensuring immediate concrete quality in a construction project. The flowability of four types of HPC was tested by a mini-slump cone which has an inside diameter of 36 mm at the top and 60 mm at the bottom, and a height of 60 mm. The testing method is followed GB/T2419-2005 (2005).

2.5.2. Static and dynamic properties

Compressive and flexural strength is a widely accepted measure to access the performance of a given concrete mixture in real-life applications. The static flexural behaviour of four types of HPC specimens was evaluated by GB/T17671-1999. Each type of HPC has three specimens. The load using the MTS tester at a displacement rate of 2 mm/min was applied. The compressive strength of HPC specimens was tested under 2.4 kN/s, according to GB/T17671-1999 (1999).

Concrete structures may be exposed to dynamic loadings such as earthquakes and vehicles load, resulting in substantial damage to human life and property because of the collapse of concrete structures. The evaluation of dynamic properties for concrete is very important when the structure uses in a vibration service environment. Dynamic mechanical behaviours are characterized by the split Hopkinson pressure bar (SHPB) (Zhang and Zhao, 2014), three-point dynamic bending test devices (Ou et al., 2008), and dynamic mechanical analyzer (DMA) (Long et al., 2018). Because the SHPB crushes the specimens, and three-point dynamic bending test devices require large specimens for testing over a long beam, these two devices require large amounts of raw materials for sufficient specimen preparation. DMA is widely used to investigate the properties of rubber, steel, fibers, and geopolymer. DMA requires only a small specimen and conduct experiment more easily. DMA was chosen to investigate the dynamic mechanical behaviour including damping property, storage modulus, energy dissipation in this study. Based on the previous experiment (Long et al., 2018), 28-day dynamic behaviour of HPC was tested at room temperature (25.3–25.5 °C), with excitation frequencies of 0.1–200 Hz. The static and dynamic force of −200 N, 100 N were used.

2.5.3. Fiber pullout testing

According to Chinese standard CECS13-2009 (2009), dog-bone shaped specimens were used to evaluate the interfacial bond properties between fiber and mortar matrix. It can reveal the enhanced mechanism of dynamical properties in HPC-LC^3. Four steel fibers with the length of 13 mm were vertically fixed at the plastic sheet by using glue. To ensure that the fibers were all pulled out from the pull-out half, the embedded length of fibers in the pull-out half and the fixed half were set to 5 mm and 8 mm, respectively. The plastic sheet was inserted into the groove in the middle of the mold and the mixture was poured. After 24 h, the specimens were demolded after 24 h casting and cured in a standard curing room for 28-day.

2.5.4. Hammer modal analysis testing

Waves in a solid generated from an external input can interfere and create standing waves if the input provides energy to the frequencies that corresponds to the solids natural frequencies. The condition of when the input frequencies equal the natural frequencies of a solid is known as resonance. The dynamic property of concrete structure was also investigated by hammer modal testing method for small size beam (8 × 10*43 mm) (Tong et al., 2002). Modal analysis of the data obtained from structural testing, provides us with a definitive description of the response of a structure. To obtain an accurate result, three piezoelectric acceleration sensor was adhesive on the simply supported beam uniformly.

According to Huang et al. (2010), the natural frequency of a simply supported beam can be calculated by the following functions:

$$W_r = r^2\pi^2\sqrt{\frac{EI}{\rho l^4}}\ (r = 1, 2, 3, \ldots. k)$$

where W_r is the natural frequency of the r-th mode; EI is stiffness; ρ is the density of beam; l is the length of the beam. In this study, the damping ratio and loss factor of the simply supported beam under 1st-mode natural frequency was used to characterized the dynamic property of concrete structure.

2.5.5. Microstructural characterization techniques

The dynamic mechanical behavior of concrete materials relates to the internal microstructure of concrete. The mercury intrusion porosimetry (MIP) and BSEM can be used to reveal the enhanced mechanism of mechanical performance by investigating the pore structure of concrete. The pore structures of HPC are tested by MIP (Dhandapani and Santhanam, 2017). After 28 d of curing, the specimens that had been subjected to DMA were crushed into particles with sizes of 3–5 mm, then soaked in acetone to stop the hydration process, and then dried in an oven at 60 °C for 24 h before examination. The MIP experiments were sequentially conducted under low and high pressures, respectively. The full-scan auto mode was selected with a contact angle and surface tension of 130° and 485 mN/m, respectively. The volume of intruded mercury was recorded at each pressure point.

Specimens (10 mm^3) for BSEM were cast into moulds filled with acrylic glue before the specimens were polished at low speed to eliminate the crack of the interfaces based on the previous experiment (Long et al., 2021). The morphology and atomic ratios of the hydration products were determined by an energy dispersive spectrometer.

2.5.6. Thermal gravimetric analyzer (TGA) and nuclear magnetic resonance spectroscopy (NMR)

The mechanical behavior of materials relates to internal microstructure of concrete. The microstructure of concrete influence by cement hydration characterization, such as hydration products and hydration degree. The SDT Q600 TGA and JNM ECZ600R NMR can be used to measure hydration products and hydration degree. The TGA was conducted using a SDT Q600 (TA Instruments) analyzer with N2 atmosphere (Long et al., 2020). TGA of the samples were performed to measure the mass of the samples at 1000 °C. A 30 mg sample of the powdered sample was heated from 20 to 1000 °C at a heating rate of 10 °C/min with an Argon stripping gas (Rigaku, Thermo plus EVO2).

Solid samples were characterized using a JNM ECZ600R NMR spectrometer (Sevelsted et al., 2013). The chemical conditions of aluminosilicate gel of samples were scanned by the ^{29}Si and ^{27}Al- NMR tests. The ^{29}Si-NMR spectra were collected at 119.2 MHz with a probe for 3.2 mm zirconia rotors and a spinning speed of 10.0 kHz. The number of scans, relaxation delay, and pulse width were 1000, 20s, and 0.1μs, respectively. All spectra were externally referenced to the ^{29}Si signal from tetramethylsilane (TMS). Deconvolution analysis of all ^{29}Si-NMR spectra was performed using the Gaussian function. The full-width at half height of each component peak was constrained to 2.50 ppm. The ^{27}Al-NMR spectra were collected at 156.4 MHz with the same instrument. The number of scans, relaxation delay, and pulse width were 32, 5s, and 0.1μs, respectively.

2.5.7. Ecological evaluation of HPC systems

In this study, embodied energy (EE), embedded CO_2 emissions (ECO_2e), and costs of HPC were estimated. The ecological evaluation was conducted by life cycle assessments based on EN ISO 14040 (2006). Although EE, ECO_2e, and costs of raw materials are often calculated for the processing, transportation, production, and curing phases. EE, ECO_2e, and costs produced during the transportation, production and curing phases were not considered in this study because their contribution to environmental burden was considered the same. The EE, ECO_2e, and costs were calculated by summing the ECO_2e in the processing and curing phases.

All embodied impacts of the relevant construction materials are shown in Table 6. Activities costs and relevant data for the various HPC specimens were based on field investigations and our own experiments. Most of relevant construction materials were obtained from EN ISO 14040 (2006), such as water, cement and silica fume. Besides, limestone is obtained from investigation by Cancio Díaz et al. (2017), and calcined clay is reported by Yu et al. (2021).

Table 6
EE, ECO_2e, and cost of basic parameters (ISO 14044:2006, 2006b; Cancio Díaz et al., 2017; Yu et al., 2021).

Components		Data for each material		
		EE (MJ/kg)	ECO_2e ($kgCO_2e$/kg)	Cost (RMB/kg)
Binder	Limestone	0.85	0.032	0.3
	Gypsum	1.80	0.12	0.2
	Calcined clay	2.734	0.196	0.45
	Ground clinker	5.5	0.74	0.75
	Silica fume	–	–	2
	Cement	5.5	0.95	0.78
Additives	Water	0.2	0.0008	0.007
	Super plasticizer	11.5	0.75	8
Aggregates	River Sand	0.081	0.0051	0.06
Fiber	Steel fiber	0.15	1.4965	10.5

Note: Parameters used to calculate cost are based on the prices of materials in Shenzhen, China.

3. Results and discussions

To develop a new-green concrete product (HPC-LC^3) with high dynamical properties and promote its mass use in a vibration service environment, the fresh performance (workability), static and dynamic properties of HPC mixed with different binder proportion will be analyzed in this section. Furthermore, the mechanism of dynamical performance will be discussed by investigating microstructure and hydration of HPC. The optimal mixture, in this section, will be recommended based on the balance between dynamic properties and environmental assessment.

3.1. Mini-slump flow of HPC

The mini-slump flow expansion was tested immediately after the different mix proportions were prepared, and the flow values are presented in Fig. 3. Compared to the reference HPC with OPC, the mini-slump flow expansion of HPC with LC^3 decreased. This indicates that higher superplasticizer requirement in HPC with LC^3 was needed to improve the slump flow. As shown in Fig. 1, the reason for this result was due to higher fineness of LC^3 as compared to the reference, which agreed with the result of Nair et al. (2020). The slump flow of HPC- LC^3 with 40%, 45% calcined clay (LC^3-45, LC^3-40) deceases by 7.7% and 11.0% in comparison with HPC with 35% calcined clay (LC^3-50). The result indicates that high dosage of calcined clay has a negative effect on the mini-slump flow of HPC. The similar mini-slump result of this study has been reported by Chen et al. (2021) (150–220 mm) and Yu et al. (2020) (160–200 mm).

As reported by Giaccio and Zerbino (2002), the saturation point of superplasticizers increases with the increase in fineness of particle size, and the higher specific surface area of calcined clay that effects the adsorption of superplasticizers. Although the mini-slump flow of HPC-LC^3 decreased in this study, the positive effect of PCE superplasticizer on the flowability of HPC-LC^3 should be recognized, which was confirmed by Li et al. (2021).

3.2. Static mechanical properties of HPC

Fig. 4 (a) shows images of the different destruction states of HPC at 28 d, after the specimens were subjected to axial compression. The damage to LC^3-40 can be seen to be particularly serious, and in this case, the compression led to slip damage due to higher dosage of calcined clay

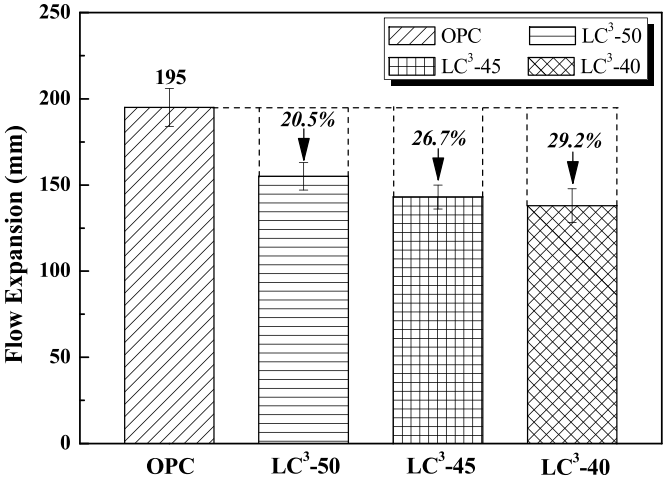

Fig. 3. Mini-slump flow of HPC.

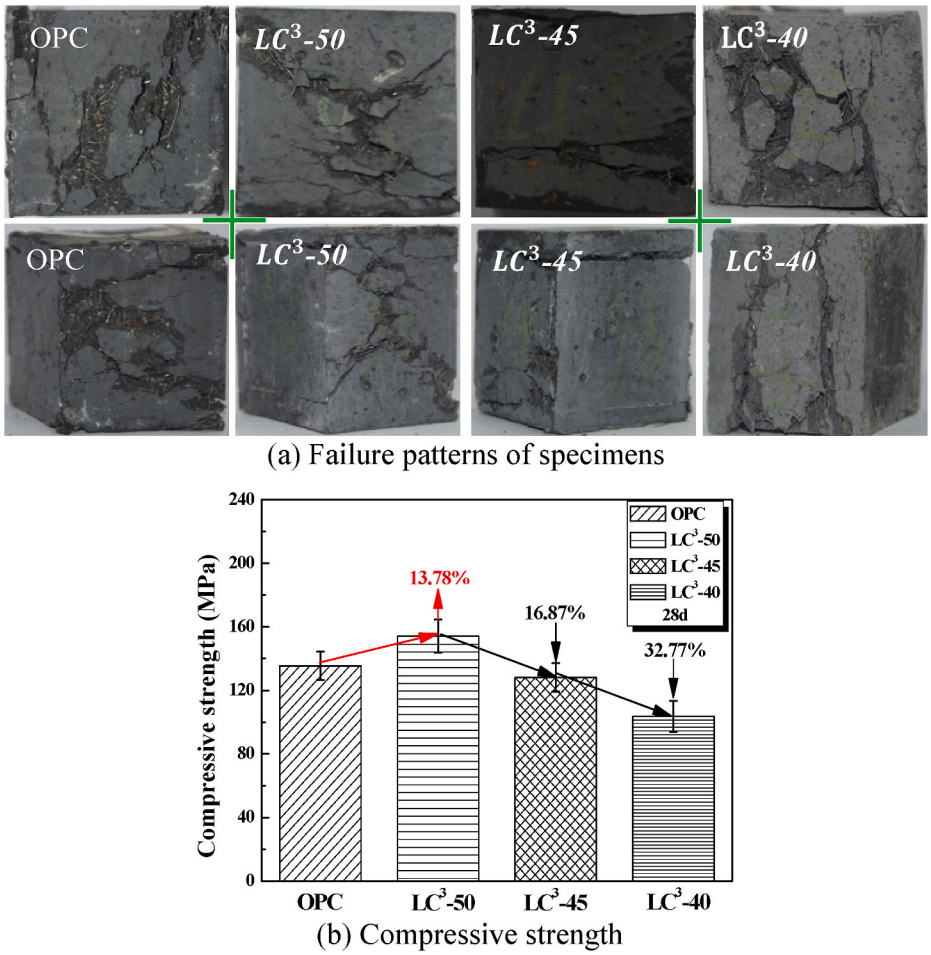

Fig. 4. Compressive strength of different HPC.

which results in the lower bond strength between fiber and matrix. The various compressive strengths of all HPC mixtures at 28 d can be seen in Fig. 4 (b). The 28-d strength of the reference specimen was 135 MPa. Compared to the reference specimen, the compressive strength of the HPC-LC^3 increased by 13.78% when the ground clinker, calcined clay was 50%, 35%. This improvement was attributed to calcined clay acting as a pore filler improved the density of matrix and the effect of better hydration characteristics of LC^3-50 binder system on the mechanical properties of concrete. The results confirm the findings reported by Dhandapani et al. (2018), indicating that the suitable dosage of calcined clay improves the mechanical properties of the matrix. The obtained higher strength was attributed to the lower porosity (Dhandapani and Santhanam, 2017), which agrees with the MIP result showed in Fig. 12 (a). The compressive strengths of LC^3-45 and LC^3-40 were 128 and 104 MPa, respectively, showing decreases of 16.87 and 32.77% in comparison with the LC^3-50. These results were attributed to the reduction of ground clinker provided a positive effect on cement hydration and high dosage of calcined clay reduced the amount of Portland and limited progressive hydration (Dhandapani and Santhanam, 2020).

As shown in Fig. 5 (a) and (b), the influence of calcined clay and

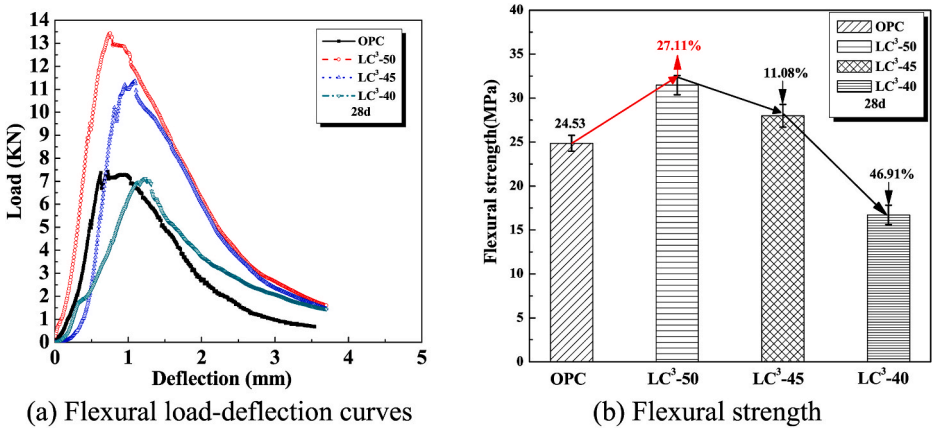

Fig. 5. Flexural behavior and failure image for HPC.

ground clinker combination on the flexural strength of HPC-LC^3 is illustrated. The flexural strengths of the four HPC mixtures initially showed similar linearity after the flexural load was applied, and then diverged to display at different peak points. LC^3-50 presented the highest load of 13430 N, followed by LC^3-45, the reference, and LC^3-40, which had peak loads of 11317, 7286, and 7126 N, respectively. This can be attributed to the higher strength of matrix, which is similar like to the compressive strength of HPC. Using high dosage of calcined clay, a low constant load was reached with a high deflection, which suggests that HPC incorporating with LC^3 offers good ductility.

Flexural strength of HPC was summarized in Fig. 5 (b). The specimen of LC^3-50 for 28-d flexural strength increased by 27% as compared to 24 MPa in the reference specimen. When the combination of ground clinker and calcined clay was 40%, 45% the flexural strength was lowest, at 16 MPa, which was lower than that of the reference specimen. This result was attributed to the lower matrix strength, which was weakened by the reduction in ground clinker and high dosage of calcined clay. This result also can be affirmed by the compressive strength.

3.3. Fiber pull-out behavior of HPC

Fig. 6 shows fiber pullout behavior of two mortars at 28-day. The pull-out load was 15 KN for LC^3-50, which was higher 15% than the pull-out of load of OPC. According to the load-slip curves, the bond strength and pullout energy of fiber embedded in different kinds of all specimen mortars can be calculated. The results show that the bond strength of fiber embedded in LC^3-50 matrix was 1.20 MPa, 10% higher than that in OPC. The bond strength result of this study shows slightly higher than the investigation by Huang et al. (2020), showing that the bond strength between fiber and matrix increases from 3% to 10%, as compared with the traditional mixture. The results of fiber pullout test indicates that the bond strength is positively related to the strength of matrix, which are consistent with the findings of compressive and flexural strength.

3.4. Dynamic mechanical behaviour of HPC

HPC is an advanced material which can be used for long-span bridge structures (Kumar and Verma, 2017), while long-span bridge structures always face different kinds of dynamical loads, such as vehicle loads, and wind loads. It is very important to investigate the dynamic mechanical behaviour of HPC because it is beneficial to understand the capability of HPC to resist dynamic load, especially the property to resist seismic waves and energy dissipation. Loss factor (tan δ), storage modulus (E′), and energy dissipation are used to characterize the dynamic mechanical behaviour of HPC (Foray-Thevenin et al., 2006). The E', tan δ, and energy dissipation of HPC are detailed in the following sections because of their importance in engineering applications of HPC-LC^3.

3.4.1. Damping property

The loss factor is the ratio of the dissipated energy to the stored energy, which shows the damping capacity of HPC (Mukherjee and Joshi, 2005). The results of the tan δ analysis for the reference, LC$_3$-50, LC^3-45, and LC^3-40 specimens are shown in Fig. 7(a). The damping capability of LC^3-40 was approximately 0.3, which was significantly lower than other specimens with different combinations of LC^3. Because of the fiber addition, damping capability of LC^3-40 was higher than that of materials investigated in other references (Liu et al., 2018), even though the minimum damping property of LC^3-40 was obtained in this study. This can also be in agreement with Zhou et al. (2020). The loss factor of the LC^3-45 specimen was highest at room temperature (25 °C), and the maximum increase in the loss factor in LC^3-45 was 46.75% compared to the reference specimen. As mentioned by Long et al. (2018), the damping property was related to the moderate porosity, non-uniform stress distribution, and the large internal surface area in the testing matrix. The loss factor of LC^3-50 was lower than LC^3-40 because of a higher compressive strength, such results were also found in the previous study by Liu et al. (2018). The loss factor of HPC was associated with both the specimen strength and porosity (Long et al., 2018). The enhanced damping property was attributed to moderate porosity and high compressive strength, which was consistent with the MIP results and mechanical properties.

According to the report by Liang and Ou (2006, 2021), the damping ratio of concrete structure modes was closed to 0.5 times loss factor for concrete materials when a shear-type reinforced concrete frame with ten stories was investigated. The damping ratio is a significant parameter for concrete structure to resist the dynamic load. The obtained result in this study compared with the previous work in the field. As shown in the Fig. 7(b), the key property of HPC-LC3, loss factor, obtained from this study shows the highest value, compared with previous literature. In this study, the maximum increase in the loss factor for HPC-LC3 was 46.75% compared to the reference specimen, which means that the increment in loss factor for the concrete materials can increase the resistance ability to dynamic load for concrete structure.

3.4.2. Analysis of storage modulus

The storage modulus shows the elastic behaviour of HPC, and it is proportional to the storing energy after one cycle. The results of storage modulus analysis for the reference, LC^3-50, LC^3-45, and LC^3-40 specimens at different times are presented in Fig. 8. Storage modulus (E') of the reference was lower than that of all HPC-LC^3 specimens at room temperature (25 °C). The maximum increase in storage modulus was 102%, in LC^3-50, compared to the reference, which is due to the incorporation of LC^3 results in more hydration products which has a

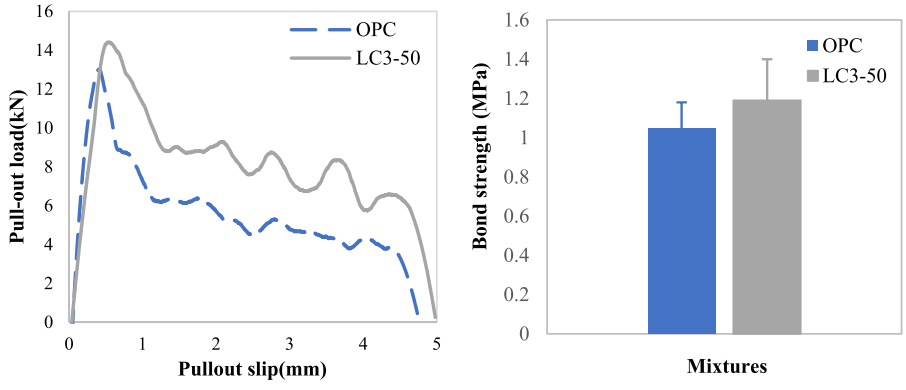

(a) Fiber pull-out curves (b) Bond strength

Fig. 6. Fiber pull-out behavior of mortars at 28-day.

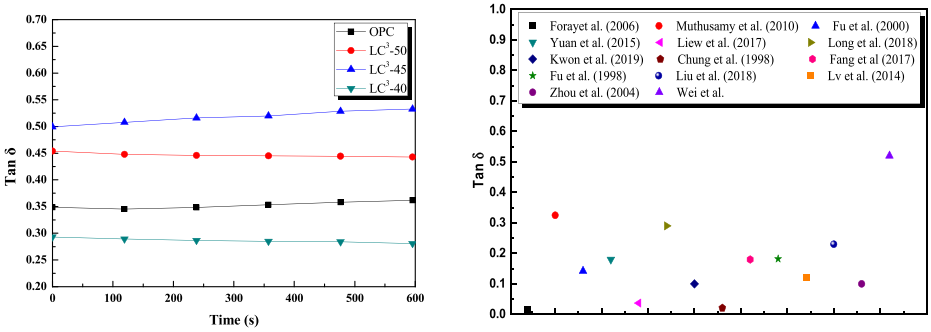

(a) Loss fator of HPC-LC^3 at 28 d (b) Loss factor in the literature

Fig. 7. The damping property of matrix materials at 28 d.

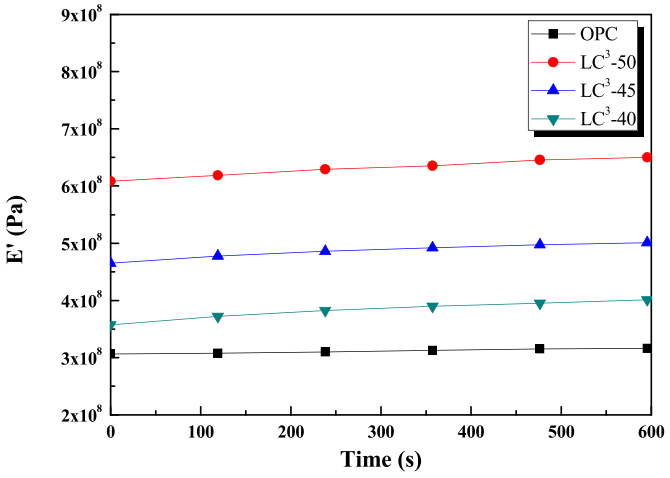

Fig. 8. DMA analysis results of storage modulus at 28 d.

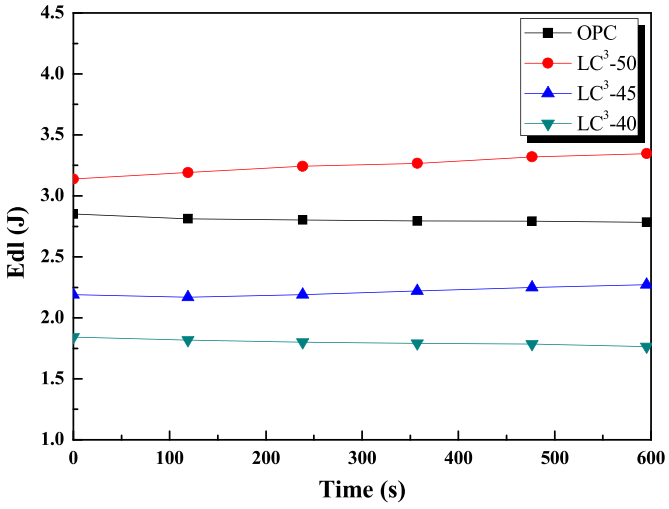

Fig. 9. DMA analysis results of energy dissipation at 28 d.

positive effect on the strengthening of the interfaces between the HPC matrix and steel fibers. This can be confirmed with the fiber pullout behavior, as shown in Fig. 6. The strengthened interfaces between matrix and the aggregate results in the storage modulus increased. The storage result of this study shows higher than the previous literature. It increased by 20% and 50%, as compared with the investigated by Lv et al. (2014) and Liu et al. (2018), respectively. The use of LC^3 was quite favorable to the storage modulus of HPC.

3.4.3. Energy dissipation

The energy dissipation represents the bond property between the steel fibers and HPC matrix: the greater the energy dissipation, the higher the deflection, such as rubber or ECC materials, can show high deflection when the concrete materials was under dynamic load. The energy dissipation of the HPC specimens upon being subjected to room temperature (25 °C) was examined, as summarized in Fig. 9. The 28-d energy dissipation of the HPC reference specimen (OPC) was approximately 2.81 J. Under dynamic conditions, the energy dissipation of LC^3-50 increased by 15.9% as compared to the reference specimen. This demonstrates that the LC^3 in HPC mixture has a positive effect on the energy dissipation. The energy dissipations from LC^3-45 and LC^3-40 were 2.21 J and 1.80 J, respectively, decreases of 21.05 and 35.86% in comparison with the reference specimen. This can be attributed to the lower bond strength between fiber and matrix, which is agreement with the flexural behavior of HPC-LC^3. The energy dissipation result of this study shows higher than the previous literature investigated by Long et al. (2018), increased by 90%. As mentioned above, energy dissipation can be indicative of the bond property between the steel fibers and HPC matrix. Because greater energy dissipation implies higher deformability, the energy dissipation parameter was considered to indicate that the deformability of LC^3-50 was the strongest among the HPC specimens. This result agreed with the flexural strength and fiber pull-out result shown in Figs. 5 and 6, as well as in the report by Meng et al. (2017).

3.5. Modal analysis

As shown in the Fig. 2, the dynamic property of concrete structure was investigated by Modal testing method for small size beam (8 × 10*43 mm). The result damping ratio of a simply support beam and loss factor of materials under natural frequency was shown in the Table 7. According to the investigation by Huang et al. (2010), the equation of the nature frequency of a simply supported beam was deduced by using Lagrange motion equation. Based on this calculation method, the natural frequency of LC^3-50 and OPC were 94.475 and 89.370 Hz, respectively. The error between the theoretical value and testing value were 2.8% and 4.5%, indicating the results can be accepted when the error was lower than 10%. The result indicates that the damping ratio of simply supported beam made with LC^3-50 was higher than that made with the reference OPC under the natural frequency, from 0.102 to 0.025. The damping ratio of both two mixtures was closed to 0.5 times loss factor of their materials, which was confirmed by the reported by Liang and Ou (2006).

3.6. Microstructural analysis

As demonstrated above, the mechanical properties of LC^3-50 were the most favorable among the mixtures with LC^3. BSEM observations of

Table 7
Modal testing result under natural frequency.

Natural Frequency				Damping ratio	Loss factor	The difference between 2 times × damping ratio and loss factor
Mix.	Theoretical result (Hz)	Testing result (Hz)	Error			
LC^3-50	94.475	97.109	2.8%	0.102	0.216	0.012
OPC	89.370	88.167	4.5%	0.025	0.043	−0.007

embedded fibers in the reference and LC^3-50 specimens were executed, as shown in Fig. 10. The figure shows several large, disconnected capillary pores in both samples. Porous microstructures around the fibers in LC^3-50 and the reference at 28 d can also be observed, the reason for that is the wall effect of steel fibers (Li et al., 1996). As observed in Fig. 10(a), it can be found that binder materials have adhered on the fiber surfaces. The reference specimen showed an obvious pore and cracking zone around the fiber, and this porous area could decrease the bond strength between the matrix and the fiber, weakening the contact strength between the matrix and the fiber over time. In LC^3-50, the fiber-matrix interface was well-bonded at 28 d more and different hydration products formed in the LC^3-50 specimen than in the reference specimen, which can be seen in Fig. 10(b).

A useful representation for discriminating among phases is a two-dimensional scatter plot of atomic ratios, such as Al/Ca and Si/Ca, which can be used to illustrate the process of generating hydration products (Rossen, 2014). Fig. 11 show the EDS analysis from BSEM images taken of regions of the reference and LC^3-50 specimens. Here, the cluster of points (100 points) is various hydration products, which contain information from C–S–H, C-A-S-H, and other Ca-bearing products. The other products are Portlandite (CH) with atomic ratios of (0.00:0.00), AFt with ratios of (0.00:0.33) and the AFm with ratios (0.00:0.50) (Rossen, 2014). Points of hydration products were located along tie-lines between the main cluster of points and the theoretical atomic ratio of a corresponding phase. As illustrated in Fig. 11, the hydration products of LC^3-50 occurred mostly between C–S–H and CH, Al_2O_3–Fe_2O_3-mono (AFm) and –tri (AFt) phases, in comparison with the reference matrix. This indicates that the mount of hydration products, such as C–S–H, AFM, and AFt, in the LC_3-50 mixture system can be detected more easily than the reference mixture. It can be attributed to the better hydration characteristics of LC^3-50 (Dhandapani et al., 2018). The results can explain the higher static and dynamic mechanical properties in the LC^3-50 as compared to the reference. Fig. 11 illustrated that CH was difficult detected in the LC^3-50 in comparison with the conference. This was attributed to calcined clays, considered as a pozzolanic material due to their siliceous and/or siliceous alumininous nature, can chemically react with CH in presence of moisture at ordinary temperatures to form compounds possessing cementitious properties. This result can also be affirmed by Mwiti et al. (2018). Consumption of CH during pozzolana reaction improves the mechanical properties and durability (Chousidis et al., 2016), which results in better static and dynamic properties of LC^3-50 than the reference.

Fig. 12 shows total porosity of different HPC at 28 d. As illustrated in Fig. 12 (a), the reference had a porosity of 9.07%. The porosity decreased by 8.13% when the cement replacement rate was 50%. This result may have occurred because calcined clay and limestone constituted a fine pore filler and generated more hydration products in comparison with the reference. With further incorporation of calcined clay combination in LC^3-45 and LC^3-40, the porosity increased by 10.83% and 14.08%, respectively, compared to OPC. Although the incorporation of limestone can fill portions of the pores in the matrix, the reduction in calcined clay and ground clinker combination also reduces the pozzolanic reactivity of HPC, which leads to fewer hydration products. These results confirm the findings of Antoni et al. (2012).

The pore diameter divides to micro-pores (<50 nm), and capillary pores (50–100 nm), macro-pores (>100 nm) (Wu et al., 2016). The pore volume distribution of LC^3 can be found in Fig. 12 (b). 28-day OPC exhibited meso-pore, capillary pore, and macro-pore volumes of 17.87,

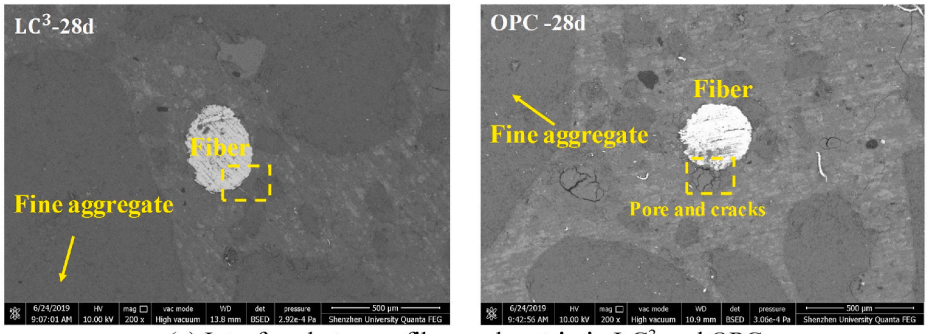

(a) Interface between fiber and matrix in LC^3 and OPC

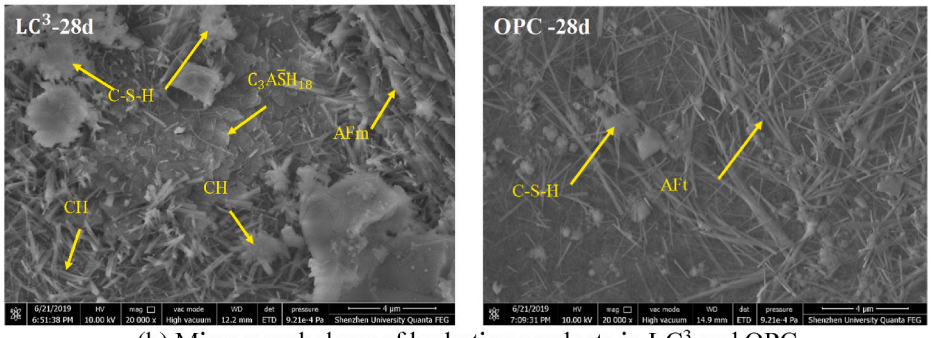

(b) Micromorphology of hydration products in LC^3 and OPC

Fig. 10. BSEM images for OPC and LC^3 matrix.

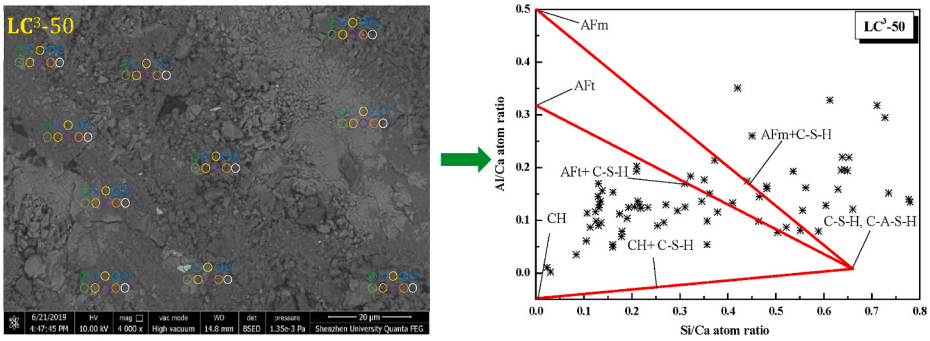

(a) LC^3-50 internal hydration products cloud map and selected points

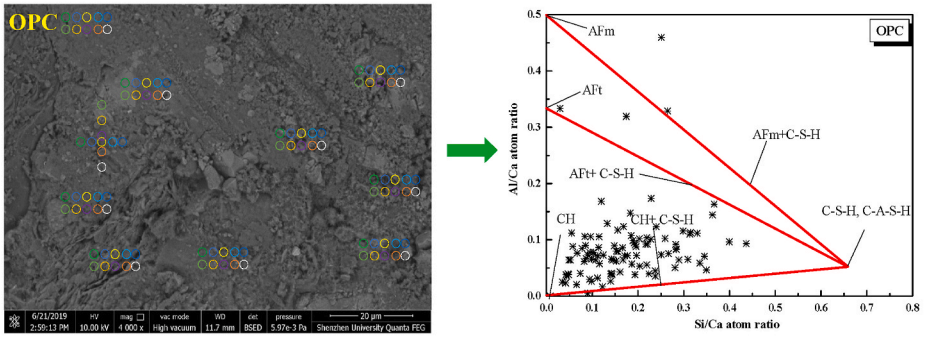

(b) OPC internal hydration products cloud map and selected points

Fig. 11. 2D scatter plots of SEM-EDS analysis, measured with 100 points.

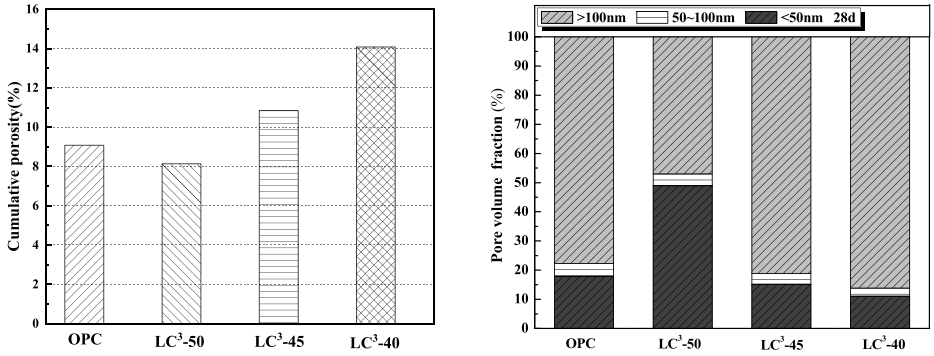

(a) The total porosity of HPC (b) Pore volume distribution of HPC

Fig. 12. MIP results of different HPC specimens.

4.43, and 77.7%, respectively. The volume of micro-pore (pore diameter <50 nm) increased with the incorporation of LC^3. The pore volume decreased with further adding limestone and reduction of calcined clay and ground clinker combination. The large capillary pore volume in LC^3-50 decreased by 20.8% compared with the reference, whereas that volume in LC^3-45 and LC^3-40 increased by 4.4 and 9.4%. The chemical reactions in HPC and bonding property between the steel fibers and matrix significantly impact the material's static and dynamic properties.

3.7. TGA analysis

Fig. 13 shows the TGA curves of the pastes at 28 days of hydration. When the temperature increases from 20 °C to 300 °C, evaporable water is released, different calcium aluminate hydrate phases become dehydrated. The evaporable water overcomes the solid phase surface adsorption constraint and becomes water vapor below 150 °C, which gradually escapes the material. Ettringite (AFt), monocarboaluminate and hemicarboaluminate, and monosulfate lose water at approximately 100 °C, 170 °C, and 190 °C (De Weerdt et al., 2011). The decomposition of C–S–H usually do not present a well-defined peak and occurs up to about 400 °C. The mass loss of LC^3-50 was higher than OPC when the temperature was between 20 °C and 300 °C, indicating better hydration characterizes in the LC^3-50. In contrast, no evident differences were observed in the CH decomposition peaks. This was attributed to CH reacted with CO_2 and then forming to $CaCO_3$. The weight loss between 600 and 800 °C is the decomposition of calcite and release of carbon dioxide to form calcium oxide. As compared to OPC, the $CaCO_3$ content in LC^3-50 was higher obviously. Lin et al. (2021) indicates the CH content in LC^3 was slightly lower than that of OPC because calcined clay consumed more CH contents as well as the formation of $CaCO_3$. This can be confirmed by the content of $CaCO_3$ in the LC^3-50.

3.8. NMR analysis

^{29}Si-NMR spectra are normally interpreted in terms of the different silicon environments and are usually denoted as Q_n, where "Q"

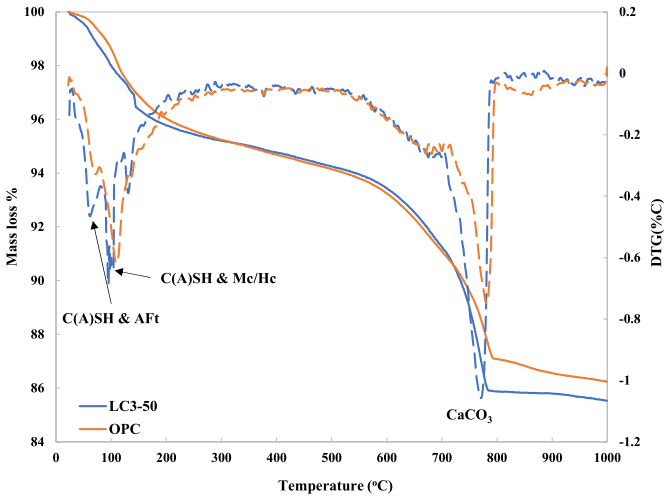

Fig. 13. TGA curves. Mass loss presented in full lines, and derivative of mass loss shown in dashed lines (Monocarboaluminate: MC; Hemicarboaluminate: HC).

represents the silicon tetrahedron bonded to four oxygen atoms and "n" denotes the number of SiO_4 units connected to the silicon tetrahedron under consideration (Massiot et al., 2002). In hydrated cement, these show the presence of Q_0 units due to orthosilicate groups, Q_1 units from Si–O–SO_3 groups in dimers or terminating polymers, and Q_2 units from Si–O–Si–O–Si groups in trimers and higher polymers.

^{29}Si-NMR spectra of the samples are shown in Fig. 14. Two spectra showed the chemical shift at 66.42–69.47 ppm (Q_0), 79.83–80.44 ppm (Q_1), 81.70–85.92 ppm(Q_2), 86.45–90.98 ppm(Q_3), and 92.95–109.38 ppm (Q_4), respectively. For each spectrum (LC^3-50 and OPC), the repartition of Q_0 to Q_4 species as a percentage of the total signal is computed, as shown in the Table 8. The Q_0 peak is indicative of unhydrated cement paste. Q_1 is the Si located at the end of C–S–H chain and Q_2 is related to the Si in the middle of C–S–H chains. Both Q_1 and Q_2 suggest the hydrated cement paste. If C–S–H could develop a net structure, Q_3 and Q_4 components are also observed in the structure. It can be observed from Table 8 that the introduction of calcined clay results in a higher degree of hydration in the LC^3-50. This can be confirmed by the investigation of Bediako et al. (2016). Another valuable observation from the spectra is the average alumina-silicate chain length (CL). It can be seen in Table 8 that the LC^3-50 causes an increase in chain length, from 3.9 to 8. The pozzolanic behavior of fine calcined clay coupled with the higher degree of hydration results in higher chain length.

Fig. 15 present the ^{27}Al NMR results of hydrated binder paste mixture of HPC mixed with OPC as well as LC^3. Two distinct ^{27}Al peaks,

Table 8
Area (%) and chain length (CL) of samples from ^{29}Si NMR spectra.

Mix.	Q_0	Q_1	Q_2	Q_3	Q_4	CL	DH (%)
LC^3-50	6.79	10.99	17.35	35.35	29.51	8	55
OPC	19.54	8.09	55.26	–	17.11	3.9	39

Note: DH, Degree of hydration (%); CL, mean alumina-silicate chain length.

around 62.76 and 4.65 ppm, were shown in the result, respectively. According to Sevelsted et al. (2013), the region between 40 and 90 ppm is assigned to the tetrahedral Al(IV) incorporated in C-A-S-H gels, while the area from 0 to 20 ppm is attributed to the octahedral Al(VI) in the hydrotalcite and/or third aluminate hydrate (TAH) phases. As shown the Fig. 15, the intensity of the Al (IV) region in the LC^3-50 samples increased significantly from 100% to 195%, as compared to the reference mixture made with OPC. The result indicates that LC^3-50 mixture can form more C-A-S-H gels after 28-day moisture curing because calcined clay in the LC^3 behaved as a filler material which accelerates the hydration (Avet et al., 2018). The acceleration of the hydration process generates more calcium hydroxide to react with the active silica and aluminate phases of pozzolans to produce secondary calcium aluminosilicate hydrates (Bediako et al., 2016). The formation of these secondary products enhances strength performance. This can be agreement with the dynamic properties and compressive strength of the mixture. Another similar conclusion can be also found in the Al (VI) phase. With the addition of calcined clay, the intensity of the Al (VI) region also increased slightly than OPC, from 100% to 121%. This can be attributed to the increment on the number of Al phases in other hydration reactions.

3.9. Ecological and economic evaluation of HPC

To investigate the application prospects of HPC-LC^3, the ecological and economic efficiency of HPC mixtures were evaluated by investigating the environmental impact and cost of each mixture. In this study, the ecological and economic efficiency of HPC-LC^3 use these parameters including the embodied energy (EE) and embodied carbon dioxide emissions (ECO_2e) of each raw material to evaluate. Most of relevant construction materials were obtained from EN ISO 14040 (2006), such as water, cement and silica fume. Besides, limestone is obtained from investigation by Cancio Díaz et al. (2017), and calcined clay is reported by Yu et al. (2021).

In this study, the EE, ECO_2e, and cost per m^3 of the HPC mixtures were calculated based on the basic values provided in Table 6. The proportion of the EE, ECO_2e, and cost for each raw material can be clearly seen in Fig. 16(a). From the reference results, the cement had the greatest impact on EE and ECO_2e, accounting for 88% of the total EE and 75% of the total CO_2 emissions, whereas the contribution of cost is small, accounting for only 21%. The findings of this study are consistent with

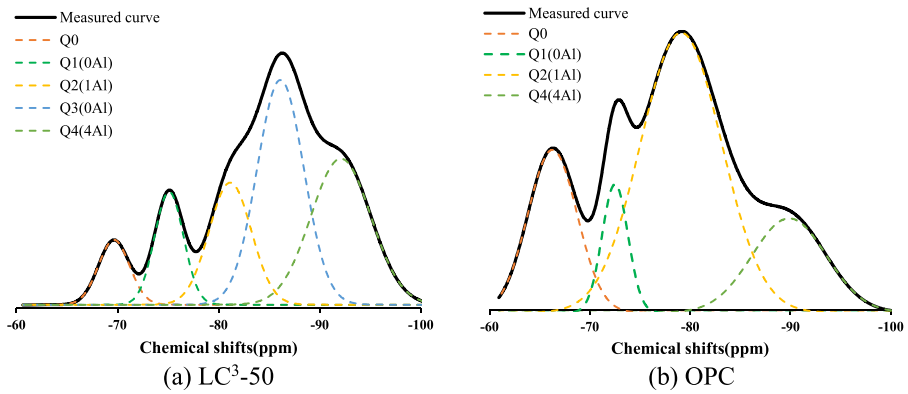

Fig. 14. ^{29}Si-NMR spectra of samples made with LC^3-50 and OPC at 28 days.

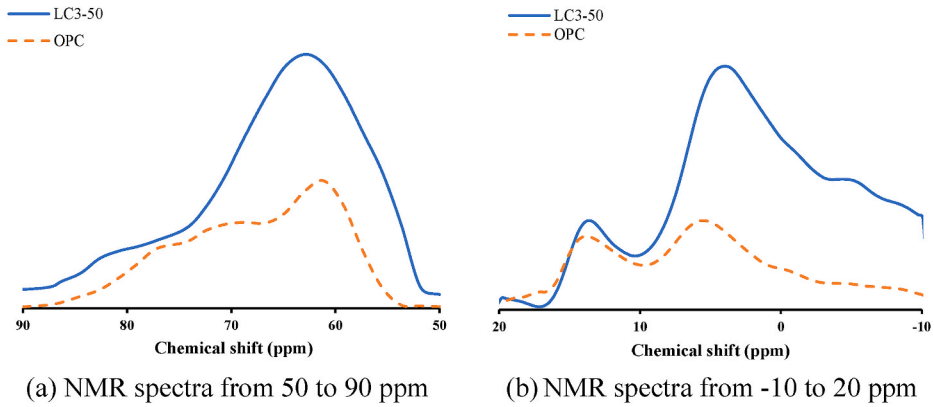

(a) NMR spectra from 50 to 90 ppm (b) NMR spectra from -10 to 20 ppm

Fig. 15. ^{27}Al-NMR spectra of LC^3-50 and OPC at 28 days.

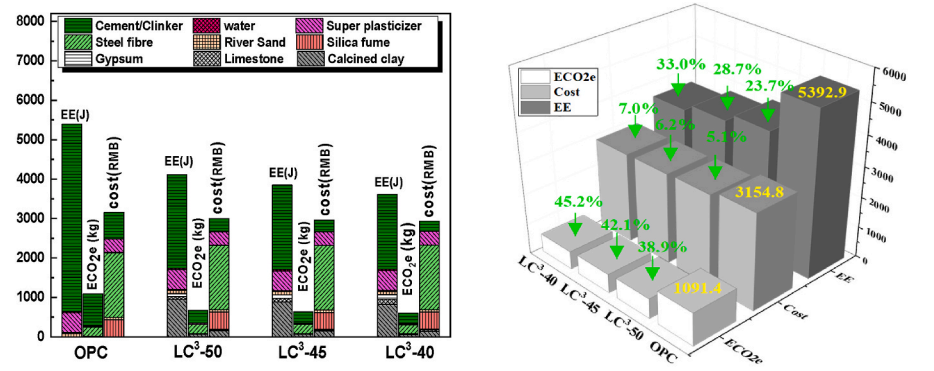

(a) EE, ECO_2e, and cost of raw materials (b) Total EE, ECO_2e, and Cost for HPC

Fig. 16. Ecological and economic efficiency of HPC-LC^3.

those in previous report (Purnell and Black, 2012). The EE and ECO_2e of the HPC-LC^3 specimens indicated that the clinker, calcined clay, and superplasticizer had the greatest impacts, accounting for 92.69 and 62.92%, 91.49 and 60.66%, and 89.19 and 58.00%, respectively. The cost of all HPC specimens was mainly influenced by the addition of fiber, accounting for 51.9–55.81%.

As shown in Fig. 16(b), there is a remarkable drop in the EE and ECO_2e of HPC with the cement replacement. The EE of the reference specimen was 5392.9 MJ/m^3, whereas the EE of LC^3-50, LC^3-45, and LC^3-40 decreased by 23.7, 28.7, and 33.0%, respectively, compared to OPC. Compared to the ECO_2e of the reference specimen, the ECO_2e of LC^3-50, LC^3-45, and LC^3-40 also decreased by 38.9, 42.1, and 45.2%, respectively. The maximum decrease was only 7.0% in the cost per m3 between OPC and the LC^3 specimens. The production of HPC-LC^3 in this study consumed less energy and produced less CO_2 emissions per m^3, in comparison with the reference specimen. Based on this analysis, compared to conventional HPC, HPC-LC^3 is more environmentally friendly and economically efficient, and the extensive use of HPC-LC^3 would promote ecological, economic, and social development.

3.10. Calcined clay for balancing dynamical properties and ecological benefits in HPC

The effect of calcined clay replacement rate on dynamic properties in HPC-LC^3 was investigated. As show in Fig. 17, when the replacement rate of calcined clay was between 0% and 45%, the loss factor and storage modulus, as well as energy dissipation was from 0.3, 3.0 × 108 Pa and 1.8 J to 0.45, 6.0 × 108 Pa, and 3.2 J. The maximum loss factor and storage modulus, as well as energy dissipation were obtained, as the

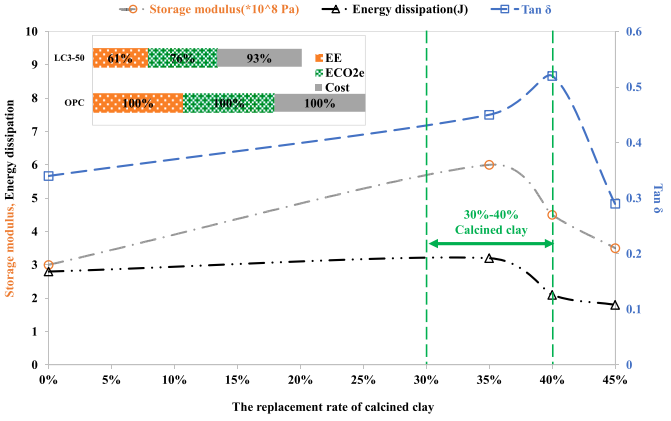

Fig. 17. Optimization replacement of calcined clay for dynamic mechanical properties and ecological performance in HPC-LC^3.

replacement rate of calcined clay was around 30%–40% in HPC-LC^3. The ecological performance of HPC-LC^3 was also in comparison with the reference, after optimizing the dosage of calcined clay. The EE, ECO_2e, and Cost in the reference herein was assumed to 100%. Compared to the reference, the EE, ECO_2e, and Cost of HPC-LC^3 with 35% calcined clay were 61%, 76%, as well as 93%, respectively. As shown in the Fig. 16 (b), the EE, ECO_2e, and Cost of HPC-LC^3 decrease by around 5%, 3%, 1%, respectively, when the replacement rate of calcined clay was from 35% to 40%. The HPC-LC^3 with 30%–40% calcined clay was recommended based on the balance between dynamic properties and

ecological benefits.

4. Conclusions

Based on the experimental results obtained in this investigation, the following conclusions can be made.

1) The mini-slump flow diameter of HPC with LC^3 decreased up by 29.2% in comparison with the reference, while the compressive and flexural strength of LC^3-50 increased by 14% and 27%, as compared to the reference. This was attributed to the increased fineness and higher pozzolanic reactivity of calcined clay.
2) Based on the DMA and modal testing results, the dynamic properties of HPC increased significantly with the addition of LC^3, compared to the reference. This enhancement was attributed to the increasing ductility of HPC and the enhancing bond strength of interface between steel fibers and matrix.
3) Based on the fiber pull-out, SEM and microstructure analysis, the interface between the steel fibers and HPC matrix was strengthened by incorporating LC^3. The total porosity of LC^3-50 at 28 d decreased by 8.13%, compared to the reference.
4) Based on the result of TGA and NMR, HPC made with LC^3-50 shows higher degree of hydration and polymerization, longer aluminasilicate chain length than that of HPC-OPC. This was attributed to that the calcined clay, acted as a fine pore filler, and promoted more hydration products, can refine pore diameter and modify the pore structure of HPC.
5) Compared to the reference, the maximum reduction in EE and ECO_2e of HPC-LC^3 were 33.0 and 45.2%. HPC-LC^3 can be considered as a novel environmentally friendly concrete. and the widespread use of HPC-LC^3 would promote sustainable environmental and economic development.
6) Based on the synthetic evaluation of dynamic properties and ecological benefits for HPC-LC^3 incorporated with different calcined clay dosage, 30%–40% calcined clay dosage in HPC-LC^3 was recommended for higher dynamic properties and lower carbon dioxide emission and energy used, as well as less cost.

This study develops a new green concrete product (HPC-LC^3) with high dynamic properties and more sustainability to promote its mass use in a vibration service environment. The application of green HPC-LC^3 in civil infrastructure reduces CO_2 emissions and improve the ability of structure for resisting dynamic loading. More research should be carried out in the future, for example, the big scale of beam used in building or slab used in pavement should be designed to validate dynamical properties of concrete materials and structure. A model should be established to evaluate dynamical properties of different structure type casted by HPC-LC^3.

CRediT authorship contribution statement

Jingjie Wei: Experimental design, Data collection, Writing – original draft. **Wu-Jian Long:** Experimental design, Supervision, and manuscript reviewing. **Kamal H. Khayat:** Writing – review & editing. **Biqin Dong:** Visualization, Investigation. **Liu Mei:** Formal analysis, and discussion, Validation. **Feng Xing:** Writing – review & editing.

Declaration of competing interest

The authors declare that they have no known competing financial interests or personal relationships that could have appeared to influence the work reported in this paper.

Acknowledgement

The authors gratefully acknowledge the financial support provided by the Science and Technology Project of Shenzhen, China (No. JCYJ20190808151011502 and No. JCYJ20180305124844894), the National Natural Science Foundations of China, NSFC-Shandong Joint Fund (No. U2006223), and the Guangdong Provincial Key Laboratory of Durability for Marine Civil Engineering (SZU) (No. 2020B1212060074), as well as Advanced Construction and Material Laboratory (ACML) and Center for Infrastructure Engineering Studies (CIES) at Missouri University of Science and Technology.

References

Alujas, A., Fernández, Rodrigo, Quintana, R., Scrivener, K., Martirena, F., 2015. Pozzolanic reactivity of low grade kaolinitic clays: influence of calcination temperature and impact of calcination products on OPC hydration. Appl. Clay Sci. 108, 94–101. https://doi.org/10.1016/j.clay.2015.01.028.

Antoni, M., Rossen, J., Martirena, F., Scrivener, K., 2012. Cement substitution by a combination of metakaolin and limestone. Cement Concr. Res. 42, 1579–1589. https://doi.org/10.1016/j.cemconres.2012.09.006.

Avet, F., Li, X., Scrivener, K., 2018. Determination of the amount of reacted metakaolin in calcined clay blends. Cement Concr. Res. 106, 40–48. https://doi.org/10.1016/j.cemconres.2018.01.009.

Bediako, M., Gawu, S.K.Y., Adjaottor, A.A., Ankrah, J.S., 2016. Early and late strength characterization of portland cement containing calcined low-grade kaolin clay. J. Eng. https://doi.org/10.1155/2016/7210891, 2016.

Cancio Díaz, Y., Sánchez Berriel, S., Heierli, U., Favier, A.R., Sánchez Machado, I.R., Scrivener, K.L., Martirena Hernández, J.F., Habert, G., 2017. Limestone calcined clay cement as a low-carbon solution to meet expanding cement demand in emerging economies. Dev. Eng. 2, 82–91. https://doi.org/10.1016/j.deveng.2017.06.001.

Chen, Y., He, S., Zhang, Y., Wan, Z., Çopuroğlu, O., Schlangen, E., 2021. 3D printing of calcined clay-limestone-based cementitious materials. Cement Concr. Res. 149, 106553 https://doi.org/10.1016/j.cemconres.2021.106553.

Chi, L., Lu, S., Yao, Y., 2019. Damping additives used in cement-matrix composites: a review. Compos. B Eng. 164, 26–36. https://doi.org/10.1016/j.compositesb.2018.11.057.

Chousidis, N., Ioannou, I., Rakanta, E., Koutsodontis, C., Batis, G., 2016. Effect of fly ash chemical composition on the reinforcement corrosion, thermal diffusion and strength of blended cement concretes. Construct. Build. Mater. 126, 86–97. https://doi.org/10.1016/j.conbuildmat.2016.09.024.

Chung, D.D.L., 2000. Cement reinforced with short carbon fibers: a multifunctional material. Compos. Part B Eng. 31 (6–7) https://doi.org/10.1016/S1359-8368(99)00071-2.

Chung, D.D.L., 2002. Review: improving cement-based materials by using silica fume. J. Mater. Sci. 37, 673–682. https://doi.org/10.1023/A:1013889725971.

De Weerdt, K., Haha, M. Ben, Le Saout, G., Kjellsen, K.O., Justnes, H., Lothenbach, B., 2011. Hydration mechanisms of ternary Portland cements containing limestone powder and fly ash. Cement Concr. Res. 41, 279–291. https://doi.org/10.1016/j.cemconres.2010.11.014.

Dhandapani, Y., Santhanam, M., 2017. Assessment of pore structure evolution in the limestone calcined clay cementitious system and its implications for performance. Cement Concr. Compos. 84, 36–47. https://doi.org/10.1016/j.cemconcomp.2017.08.012.

Dhandapani, Y., Santhanam, M., 2020. Influence of calcined clay-limestone ratio on properties of concrete with limestone calcined clay cement (LC^3). In: Bishnoi, S. (Ed.), Calcined Clays for Sustainable Concrete. Springer Singapore, Singapore, pp. 731–738. https://doi.org/10.1007/978-981-15-2806-4_81.

Dhandapani, Y., Sakthivel, T., Santhanam, M., Gettu, R., Pillai, R.G., 2018. Cement and concrete research mechanical properties and durability performance of concretes with limestone calcined clay cement (LC3). Cement Concr. Res. 107, 136–151. https://doi.org/10.1016/j.cemconres.2018.02.005.

Fang, L., Yuan, Q., Deng, D., Pan, Y., Wang, Y., 2017. Effect of mix parameters on the dynamic mechanical properties of cement asphalt mortar. J. Mater. Civ. Eng. 29, 04017080 https://doi.org/10.1061/(asce)mt.1943-5533.0001913.

Foray-Thevenin, G., Vigier, G., Vassoille, R., Orange, G., 2006. Characterization of cement paste by dynamic mechanical thermo-analysis: Part I: operative conditions. Mater. Char. 56, 129–137. https://doi.org/10.1016/j.matchar.2005.10.007.

Fu, X., Chung, D.D.L., 1996. Vibration damping admixtures for cement. Cement Concr. Res. 26, 69–75. https://doi.org/10.1016/0008-8846(95)00177-8.

Fu, X., Li, X., Chung, D.D.L., 1998. Improving the vibration damping capacity of cement. J. Mater. Sci. 33, 3601–3605. https://doi.org/10.1023/A:1004603312273.

GB/T 14684-2011, 2011. Sand standard for construction. Building Materials Industry Technology Supervision and Research Center of the People's Republic of China, Beijing.

GB/T 175-2007, 2007. Common Portland Cement. People's Republic of China, Beijing.

Giaccio, G., Zerbino, R., 2002. Optimum superplasticizer dosage for systems with different cementitious materials. Indian Concr. J. 76, 553–557.

Gursel, A.P., Maryman, H., Ostertag, C., 2016. A life-cycle approach to environmental, mechanical, and durability properties of "green" concrete mixes with rice husk ash. J. Clean. Prod. 112, 823–836. https://doi.org/10.1016/j.jclepro.2015.06.029.

Huang, Y., Zhao, Y., Zhao, W., 2010. Analysis on the natural frequency of a simply supported beam. J. Qinghai Univ. (Nature Sci.) 6, 20–31.

Huang, Z., Huang, Y., Liao, W., Han, N., Zhou, Y., Xing, F., Sui, T., Wang, B., Ma, H., 2020. Development of limestone calcined clay cement concrete in South China and

its bond behavior with steel reinforcement. J. Zhejiang Univ. 21, 892–907. https://doi.org/10.1631/jzus.A2000163.
ISO 14044:2006. Geneva, Switzerland: International Organization for Standardization; 2006b..
JG/T 223-2007, 2007. Polycarboxylates High Performance Water-Reducing Admixture. Chinese construction industry standard, Beijing.
Kumar, A., Verma, B., 2017. High performance concrete and its applications in civil ENGG. Int. J. Adv. Res. Sci. Eng. 470–477, 06.
Kwon, S., Ahn, S., Koh, H.-I., Park, J., 2019. Polymer concrete periodic meta-structure to enhance damping for vibration reduction. Compos. Struct. 215, 385–390. https://doi.org/10.1016/j.compstruct.2019.02.022.
Li, V., Wu, H., Chan, Y., 1996. Effect of plasma treatment of polyethylene fibers on interface and cementitious composite properties. J. Am. Ceram. Soc. 79, 700–704. https://doi.org/10.1111/j.1151-2916.1996.tb07932.x.
Li, R., Lei, L., Sui, T., Plank, J., 2021. Effectiveness of PCE superplasticizers in calcined clay blended cements. Cement Concr. Res. 141, 106334. https://doi.org/10.1016/j.cemconres.2020.106334.
Liang, C., Ou, Jinping, 2006. Relationship between structural damping and material damping. Earthq. Eng. Eng. Vib. 26, 44–55.
Liew, K.M., Kai, M.F., Zhang, L.W., 2017. Mechanical and damping properties of CNT-reinforced cementitious composites. Compos. Struct. 160, 81–88. https://doi.org/10.1016/j.compstruct.2016.10.043.
Lin, R.-S., Han, Y., Wang, X.-Y., 2021. Macro–meso–micro experimental studies of calcined clay limestone cement (LC^3) paste subjected to elevated temperature. Cement Concr. Compos. 116, 103871. https://doi.org/10.1016/j.cemconcomp.2020.103871.
Liu, T., Song, W., Zou, D., Li, L., 2018. Dynamic mechanical analysis of cement mortar prepared with recycled cathode ray tube (CRT) glass as fine aggregate. J. Clean. Prod. 174, 1436–1443. https://doi.org/10.1016/j.jclepro.2017.11.057.
Long, W., Wei, J., Xing, F., Khayat, K., 2018. Enhanced dynamic mechanical properties of cement paste modified with graphene oxide nanosheets and its reinforcing mechanism. Cement Concr. Compos. 93, 127–139. https://doi.org/10.1016/j.cemconcomp.2018.07.001.
Long, W.J., Ye, T.H., Xing, F., Khayat, K.H., 2020. Decalcification effect on stabilization/solidification performance of Pb-containing geopolymers. Cement Concr. Compos. 114, 103803. https://doi.org/10.1016/j.cemconcomp.2020.103803.
Long, W.J., Li, H.D., Mei, L., Li, W., Xing, F., Khayat, K.H., 2021. Damping characteristics of PVA fiber-reinforced cementitious composite containing high-volume fly ash under frequency-temperature coupling effects. Cement Concr. Compos. 118, 103911. https://doi.org/10.1016/j.cemconcomp.2020.103911.
Lv, S., Ting, S., Liu, J., Zhou, Q., 2014. Use of graphene oxide nanosheets to regulate the microstructure of hardened cement paste to increase its strength and toughness. CrystEngComm 16, 8508–8516. https://doi.org/10.1039/C4CE00684D.
Massiot, D., Fayon, F., Capron, M., King, I., Le Calvé, S., Alonso, B., Durand, J., Bujoli, B., Gan, Z., Hoatson, G., 2002. Modelling one-and two-dimensional solid-state NMR spectra. Magn. Reson. Chem. 40, 70–76. https://doi.org/10.1002/mrc.984.
Meng, W., Yao, Y., Mobasher, B., Khayat, K.H., 2017. Effects of loading rate and notch-to-depth ratio of notched beams on flexural performance of ultra-high-performance concrete. Cement Concr. Compos. 83, 349–359. https://doi.org/10.1016/j.cemconcomp.2017.07.026.
Meng, W., Khayat, K.H., Bao, Y., 2018. Flexural behaviors of fiber-reinforced polymer fabric reinforced ultra-high-performance concrete panels. Cement Concr. Compos. 93, 43–53. https://doi.org/10.1016/j.cemconcomp.2018.06.012.
Mukherjee, A., Joshi, M., 2005. FRPC reinforced concrete beam-column joints under cyclic excitation. Compos. Struct. 70 (2), 185–199. https://doi.org/10.1016/j.compstruct.2004.08.022.
Muthusamy, S., Wang, S., Chung, D.D.L., 2010. Unprecedented vibration damping with high values of loss modulus and loss tangent, exhibited by cement–matrix graphite network composite. Carbon N. Y. 48, 1457–1464. https://doi.org/10.1016/j.carbon.2009.12.040.
Mwiti, M.J., Karanja, T.J., Muthengia, W.J., 2018. Properties of activated blended cement containing high content of calcined clay. Heliyon 4, e00742. https://doi.org/10.1016/j.heliyon.2018.e00742.
Nair, N., Mohammed Haneefa, K., Santhanam, M., Gettu, R., 2020. A study on fresh properties of limestone calcined clay blended cementitious systems. Construct. Build. Mater. 254, 119326. https://doi.org/10.1016/j.conbuildmat.2020.119326.
Nguyen, Q.D., Kim, T., Castel, A., 2020. Mitigation of alkali-silica reaction by limestone calcined clay cement (LC3). Cement Concr. Res. 137, 106176. https://doi.org/10.1016/j.cemconres.2020.106176.
Ou, J., Liu, T., Li, J., 2008. Dynamic and seismic property experiments of high damping concrete and its frame models. J. Wuhan Univ. Technol. Sci. Ed. - J. Wuhan Univ. Technol-Mater. SCI 23, 1–6. https://doi.org/10.1007/s11595-006-1001-5.
Purnell, P., Black, L., 2012. Embodied carbon dioxide in concrete: variation with common mix design parameters. Cement Concr. Res. 42, 874–877. https://doi.org/10.1016/j.cemconres.2012.02.005.
Rossen, J., 2014. Composition and Morphology of C-A-S-H in Pastes of Alite and Cement Blended with Supplementary Cementitious Materials. https://doi.org/10.5075/epfl-thesis-6294.
Scrivener, K., Martirena, F., Bishnoi, S., Maity, S., 2018. Calcined clay limestone cements (LC3). Cement Concr. Res. 114, 49–56. https://doi.org/10.1016/j.cemconres.2017.08.017.
Sevelsted, T.F., Herfort, D., Skibsted, J., 2013. 13C chemical shift anisotropies for carbonate ions in cement minerals and the use of 13C, 27Al and 29Si MAS NMR in studies of Portland cement including limestone additions. Cement Concr. Res. 52, 100–111. https://doi.org/10.1016/j.cemconres.2013.05.010.
Snellings, R., 2016. Assessing, understanding and unlocking supplementary cementitious materials. RILEM Tech. Lett. 1, 50. https://doi.org/10.21809/rilemtechlett.2016.12.
Tong, J.-H., Wu, T.-T., Lee, C.-K., 2002. Fabrication of a piezoelectric impact hammer and its Application to the in-situ nondestructive evaluation of concrete. Jpn. J. Appl. Phys. 41 https://doi.org/10.1143/JJAP.41.6595.
Wang, X., Shui, Z., Zhao, Z., Song, Q., Yang, B., Fan, D., 2018. Development of a novel cleaner construction product: ultra-High Performance Concrete incorporating lead-zinc tailings. J. Clean. Prod. 196 https://doi.org/10.1016/j.jclepro.2018.06.058.
Wu, Z., Shi, C., Khayat, K.H., 2016. Influence of silica fume content on microstructure development and bond to steel fiber in ultra-high strength cement-based materials (UHSC). Cement Concr. Compos. 71, 97–109. https://doi.org/10.1016/j.cemconcomp.2016.05.005.
Yang, P., Dhandapani, Y., Santhanam, M., Neithalath, N., 2020. Simulation of chloride diffusion in fly ash and limestone-calcined clay cement (LC3) concretes and the influence of damage on service-life. Cement Concr. Res. 130, 106010 https://doi.org/10.1016/j.cemconres.2020.106010.
Yu, J., Wu, H.L., Leung, C.K.Y., 2020. Feasibility of using ultrahigh-volume limestone-calcined clay blend to develop sustainable medium-strength Engineered Cementitious Composites (ECC). J. Clean. Prod. 262, 121343 https://doi.org/10.1016/j.jclepro.2020.121343.
Yu, J., Wu, H.L., Mishra, D.K., Li, G., Leung, C.K., 2021. Compressive strength and environmental impact of sustainable blended cement with high-dosage Limestone and Calcined Clay (LC2). J. Clean. Prod. 278, 123616 https://doi.org/10.1016/j.jclepro.2020.123616.
Yuan, X., Liu, X., Zuo, J., 2015. The development of new energy vehicles for a sustainable future: a review. Renew. Sustain. Energy Rev. 42, 298–305. https://doi.org/10.1016/j.rser.2014.10.016.
Yuan, Q., Liu, W., Pan, Y., Deng, D., Liu, Z., 2016. Characterization of cement asphalt mortar for slab track by dynamic mechanical thermoanalysis. J. Mater. Civ. Eng. 28, 04015154 https://doi.org/10.1061/(asce)mt.1943-5533.0001401.
Zhang, Q.B., Zhao, J., 2014. A review of dynamic experimental techniques and mechanical behaviour of rock materials. Rock Mech. Rock Eng. 47, 1411–1478. https://doi.org/10.1007/s00603-013-0463-y.
Zhou, Z., Zhang, S., Wang, C., Zuo, J., He, Q., Rameezdeen, R., 2016. Achieving energy efficient buildings via retrofitting of existing buildings: a case study. J. Clean. Prod. 112, 3605–3615. https://doi.org/10.1016/j.jclepro.2015.09.046.
Zhou, C., Pei, X., Li, W., Liu, Y., 2020. Mechanical and damping properties of recycled aggregate concrete modified with air-entraining agent and polypropylene fiber. Materials 13. https://doi.org/10.3390/MA13082004.